MRI Reconstruction Using Discrete Fourier Transform: A tutorial

Abiodun M. Aibinu, Momoh J. E. Salami, Amir A. Shafie and Athaur Rahman Najeeb

***Abstract*—**The use of Inverse Discrete Fourier Transform (IDFT) implemented in the form of Inverse Fourier Transform (IFFT) is one of the standard method of reconstructing Magnetic Resonance Imaging (MRI) from uniformly sampled K-space data. In this tutorial, three of the major problems associated with the use of IFFT in MRI reconstruction are highlighted. The tutorial also gives brief introduction to MRI physics; MRI system from instrumentation point of view; K-space signal and the process of IDFT and IFFT for One and two dimensional (1D and 2D) data.

***Keywords*—**Discrete Fourier Transform (DFT), K-space Data, Magnetic Resonance (MR), Spin, Windows.

I. Introduction

Magnetic Resonance Imaging (MRI) is based on the principles of tomographic imagine technique [1]–[3]. It is used primarily in medical fields to produce images of the internal structure of human body. MRI provides more diagnostic information than any of the existing imaging techniques, moreso, it does not involve the use of ionizing radiation hence, free from associated harmful effects known with other imaging techniques [4].

MRI imaging equation can be express as a two dimensional entity given as

$$S(k_x, k_y) = f[I(x, y)] \tag{1}$$

where f represent spatial information encoding scheme [1]. If f is invertible, a data consistent I can be obtained from the inverse transform such that

$$I(x, y) = f^{-1}S(k_x, k_y) \tag{2}$$

The desired image intensity function I(x,y) is a function of: Relaxation times, $T1$, $T2$ and $T2^*$; spin density, ρ; Diffusion coefficients D and so on [3]. Using function notation, this can be written as

$$I = f[T1, T2, T2^*, \rho, D] \tag{3}$$

Generally, T_1 and T_2 are two independent processes and happen simultaneously. T_1 is called spin lattice relaxation, because the energy from this process is released to the surrounding tissue (lattice) [1], [2], [4]. T_1 happens along the z-component axis and its value is always greater than the spin-spin relaxation T_2. The relationship between protons and their immediate surroundings (molecules) is describe by the spin-spin relaxation T_2 and it happens along x-y plane [1]–[4].

Athaur Rahman Najeeb is with the Kulliyah of Engineering, International Islamic University Malaysia (IIUM), email: athaur@iiu.edu.my
Momoh. J. E Salami is with the Kulliyah of Engineering, International Islamic University Malaysia (IIUM), email: momoh@iiu.edu.my
Amir A. Shafie is with the Kulliyah of Engineering, International Islamic University Malaysia (IIUM), email: aashafie@iiu.edu.my
Abiodun. M. Aibinu, Malaysia, email: maibinu@gmail.com

II. Some Basic Terminologies in MRI

- **Spin**
  Spin is a fundamental property of nature like electrical charge or mass and comes in multiples of 1/2 [4]. Spin can either be positive (+) on negative (-) and is present in protons, electrons, and neutrons. Two or more particles with spins having opposite signs can pair up to eliminate the observable manifestations of spin. In Nuclear magnetic resonance (NMR), it is unpaired nuclear spins that are of importance and nuclei with a nonzero spins are regarded as a microscopic magnet [4], [5].
- **Spin Resonance Equation**
  When spins are placed in a magnetic field of strength (**B**), they exhibit resonance at a well-defined frequency, called the Larmor frequency (υ) [1], [4], [5]. The equation governing this is
  $$\upsilon = \gamma B \tag{4}$$
  Where γ is the gyromagnetic ratio of the particle.
- **Energy Level**
  The spin vector of a particle align itself with the external magnetic field to create two distinct energy states namely, the low energy level and the high energy level [1], [2], [4]. A particle in the low energy state can absorb photons and ends up in the high energy state. The energy absorbs must exactly match the energy difference between the two states. The energy of a photon is related to its frequency by
  $$E = h\upsilon \tag{5}$$
  Where h is the planks constant and υ is the Larmor frequency. Therefore,
  $$E = h\gamma B \tag{6}$$
- **Net Magnetization**
  In order to activate the macroscopic magnetism in an object, the object can be exposed to a strong external magnetic field B_o. This aligns all the various spins along the direction of the applied external field B_o (along the z-direction) to create a net magnetic moment M_o. Therefore, the net magnetization can be describe as the vector sum of all tiny magnetic fields of each proton pointing in the same direction as the system's magnetic field. The net magnetization and the external field B_o points in the z-direction and is now called Longitudinal

magnetization M_z. At this time, the transverse component is zero. i.e $M_{xy} = 0$.

- **Spin Echo Relaxation T_1 Processes**
  The direction of M_o can be changed by exposing the nuclear spin system to energy of a frequency equal to the energy difference between the spin states. If enough energy is put into the system, M_z can be made to lie in the x-y plane by the application of RF field B_1 [1], [4]. This external force, excite these spins out of equilibrium and tip M_o away from the z-axis (the direction of B_o), creating a measurable (nonzero) transverse component M_{xy}. The time constant which describes how M_z returns to its equilibrium value is called the spin lattice relaxation time (T_1). The equation governing this behavior as a function of the time 't' after its displacement is [4]:

$$M_z = M_o(1 - e^{-t/T_1}) \tag{7}$$

- **Spin Spin Relaxation T_2 Processes**
  If the net magnetization is placed in the x-y plane, it will rotate about the Z axis at a frequency equal to the Larmor frequency. Apart from rotation, the M_z (transverse magnetization) starts to de-phase because each of the spin packets is experiencing different magnetic field which is due to the variation in B_o field [1], [4]. The time constant which describes the return to equilibrium of the transverse magnetization, M_{xy}, is called the spin-spin relaxation time, T_2. On completion of these processes, the Net magnetization is now back along M_z axis aligned with the B_o field with the protons spinning out of phase, the situation before excitation.

III. MRI Systems

In obtaining MRI images, object to be imaged are placed in a strong magnetic field that align and de-align certain atoms in such an object. The process of alignment and de-alignment results in the emission and absorption of energy in the RF range of the electromagnetic. A typical MRI scanner is as shown in Fig. 1.

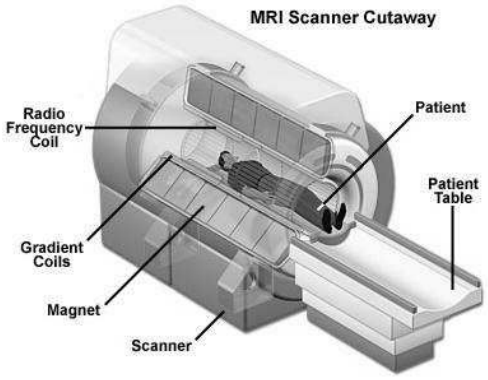

Fig. 1. Typical MRI Scanner [10]

From instrumentation point of view, An MRI scanner is made up of four main hardware components namely :

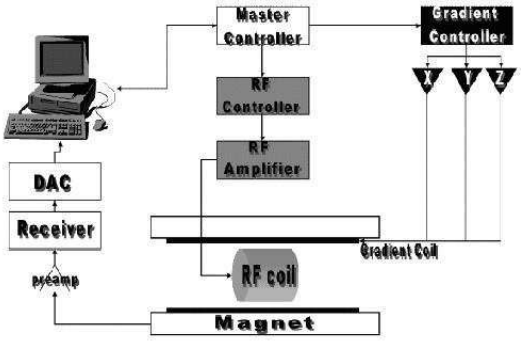

Fig. 2. MRI System from Instrumentation point of view [11]

1) **Permanent magnet**
   The main (permanent) magnet generates a strong uniform static field, referred to as the B_o field, for polarization of nuclear spins in an object.
2) **Magnetic Field Gradient System**
   The magnetic field gradient system normally consists of three orthogonal gradient coils, G_x, G_y and G_z and are essential needed for signal localization.
3) **Radio-Frequency (RF) System**
   The RF system consists of a transmitter coil, RF subsystem of RF amplifier, RF Controller and other components. This system generates a rotating magnetic field, B_1, for exciting a spin system [11], [13].
4) **Computer/Reconstruction System**
   The computer/reconstruction system converts and reconstruct the output of the receiver coil. The receiver coil converts a precessing magnetization into an electrical signal for display [11]. Most often, the process of converting the magnetization to electrical signal is often represented with a signal flow sequence.

IV. MRI Data Acquisition and K-Space data

A. MRI Data Acquisition

MRI data acquisition involves three major steps namely

1) **Gz, Slice selection by the use of Gz gradient:** This select axial slice in the object to be imaged.
2) **Gy, Phase encoding using the Gy gradient:** This creates rows with different phases.
3) **Gx, Frequency encoding using the Gx gradient:** This will create columns with different frequencies.

The K-Space is filled one line at a time, so the whole process of slice encoding, phase encoding and frequency encoding has to be repeated many times (till the whole area or slice to be image is complete).

The sampled data (data obtained by sampling the FID field) can be filled into the k-space matrix by any of the following method namely linear (Rectilinear), and other non Rectilinear methods like centric spiral, reversed centric etc [3]. Most of the available MRI scanner uses linear (rectilinear) method of filling the k-space because of the availability of FFT for reconstruction of the k-space data. Worthy of mentioning that

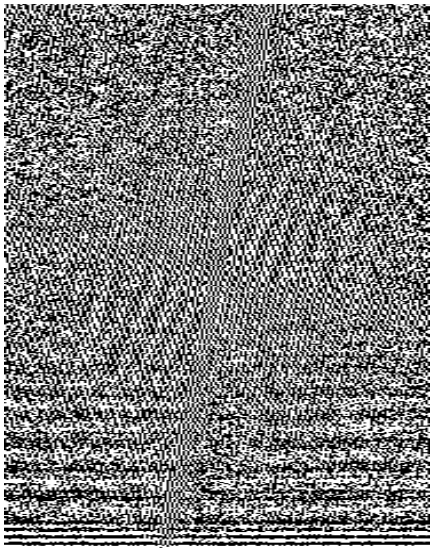

Fig. 3. Uniformly sampled K-SPACE data

rectilinear scan are not immune to artifacts, but such artifacts are well controlled and easily identifiable .

B. K-Space Data

The FID signal is sampled to obtain the discrete time like signal called k-space data. The K-space data contains all the necessary information required to reconstruct an image. Also, it gives a comprehensive way for classification and understanding of the imaging properties and method of reconstruction [13], [15].

Sampling of the acquired signal in MRI takes place in the Fourier space. The k-space data is arranged with low frequencies signals are at the center of the acquired data and the high frequencies data are spaced around this center. The low frequencies signals contain information about contrast giving the greatest changes in grey level with highest amplitude value. High frequencies signals contain information about the spatial resolution of the object or what is normally referred to as sharpness [13]. High frequency signals display rapid changes of image signal as a function of position. Fig. 3 shows a typical Uniformly sampled K-space data.

V. Image Reconstruction types

There exist various methods of converting the acquired K-space data to real images in spatial domain. These include: the use of DFT, Radon Transform, Parametric technique, Artificial neural network based reconstruction technique and so on. DFT technique involve the application of Fourier series on the linearly or radially sampled k-space data. Radon transform involve the use of projection in obtaining the required images. Parametric approach (a non Fourier series) involves implicit or explicit data extrapolation to recover some of the unmeasured (presumably lost) high-spatial-frequency data. Some of the most widely used parametric technique includes, Autoregressive (AR), Moving Average (MA), Autoregressive Moving average (ARMA) model [1]–[4], [6], [8], [9]. Other type of reconstruction that makes use of data extrapolation is the use of Artificial Neural Network technique [18]–[20].

A. Discrete Fourier Transform (DFT)

The DFT technique is used to calculate the frequency contents of a sampled signal [1]. The signal can be from any source with a periodical or suspected periodical behavior. It can also be used to analyze a non periodic signal.

The One dimensional (1D) DFT of a signal $x[n]$ is a sequence defined over the interval from [$0 : N-1$] and is given by

$$X(k) = X(2\pi\frac{k}{N}) = \sum_{n=0}^{N-1} x[n]e^{-j2\pi\frac{k}{N}} \tag{8}$$

where $k = 0, 1, 2, \ldots, N-1$. The corresponding Inverse Discrete Fourier Transform **(IDFT)** of the sequence $X(k)$ gives a sequence $x[n]$ defined on the interval [$0 : N-1$] as

$$x[n] = \frac{1}{N}\sum_{k=0}^{N-1} X[k]e^{j2\pi\frac{k}{N}} \tag{9}$$

Applying this to an image I(x,y) of size M x N gives

$$S(k_x, k_y) = \sum_{x=0}^{M-1}\sum_{y=0}^{N-1} I[x,y]e^{-j2\pi(\frac{k_x x}{M}+\frac{k_y y}{N})} \tag{10}$$

The two-dimensional (2D) DFT is given by

$$I(x,y) = \frac{1}{MN}\sum_{x=0}^{M-1}\sum_{y=0}^{N-1} S[k_x, k_y]e^{j2\pi(\frac{k_x x}{M}+\frac{k_y y}{N})} \tag{11}$$

where the variables k_x, k_y are frequency variables and x,y are spatial variables.

The fourier spectrum $|S(k_x, k_y)|$, phase angle, $\phi(k_x, k_y)$ and the power spectrum $P(k_x, k_y)$ are given as

$$|S(k_x, k_y)| = [R^2(k_x, k_y) + I^2(k_x, k_y)] \tag{12}$$

$$\phi(k_x, k_y) = \tan^{-1}[\frac{R(k_x, k_y)}{I(k_x, k_y)}] \tag{13}$$

and

$$P(k_x, k_y) = |S(k_x, k_y)|^2 \tag{14}$$

$$= R^2(k_x, k_y) + I^2(k_x, k_y) \tag{15}$$

where $R(k_x, k_y)$ and $I(k_x, k_y)$ are the real and imaginary part of $S(k_x, k_y)$ respectively.

One of the important properties of DFT is separability. The standard 2-DFT equation can be expressed in the separable 1D form as

$$S(k_x, k_y) = \sum_{x=0}^{M-1} e^{-j2\pi\frac{k_x x}{M}} \sum_{y=0}^{N-1} I[x,y]e^{-j2\pi\frac{k_y y}{N}}$$

$$= \sum_{x=0}^{M-1} S[x, k_y]e^{-j2\pi\frac{k_y y}{N}} \tag{16}$$

where

$$S(x,k_y) = \sum_{y=0}^{N-1} I[x,y] e^{-j2\pi \frac{k_y y}{N}} \quad (17)$$

From Eqn. 16, the 2-DFT of an image is equivalent to computing a 1-DFT transform along the row of the input data and then another 1-DFT transform along each of the column of the intermediate result obtained [14]

B. Application of Inverse FFT to K-Space Data

MRI reconstruction using FFT/IFFT is done in two steps, firstly the ID- IFFT of the row data is computed followed by the 1D-IFFT of column data . The same result will be obtained when 1D IFFT of the column is first computed before computing the 1D-IFFT of the column data. Reasons for this is because of linear and separability properties of DFT and the separability property discussed in section V-A and the figure is as shown in Fig. 4.

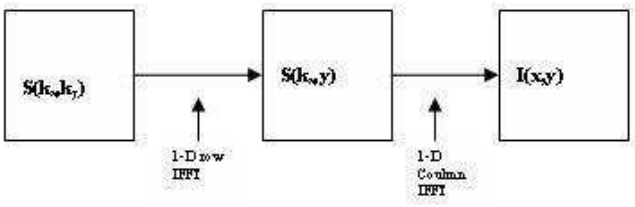

Fig. 4. 2D IFFT as cascade of 2 by 1D-IFFT

In practical MRI reconstruction, there are some other pre-processing activities that must be accomplished before the application of IFFT. The flow diagram for an MRI reconstruction is as shown in in fig. 5 and the reconstruction algorithm is discussed herewith.

- **Step 1**: Read data header information: Load RAW-nmn contain information about the MRI data file. It is a text file containing Information about Offset, DATA size, Kx Co-ordinate, Ky-Co-ordinate etc.
- **Step 2**:Read in the K-space information.
- **Step 3**: IFFT in Kx Direction ,
- **Step 4**: IFFT in Ky Direction
- **Step 5**: IFFT shift
- **Step 6**: Image Display

VI. Challenges of DFT based MRI Reconstruction

The problems associated with DFT technique of MRI reconstruction include:

- Gibb's effect around edges
- Introduction of artifacts
- Decrease in spatial resolution

A. **Gibb's effect**

The use of DFT for MRI reconstruction sometimes creates spurious ringing around sharp edges [6], [7], [9], [15]. This phenomenon is popularly known as Gibb's effect. The ringing effect around edges is due to the finite data sequence of MRI.

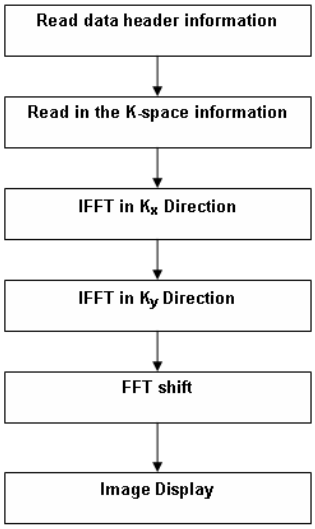

Fig. 5. Flow diagram of IFFT Method of reconstruction

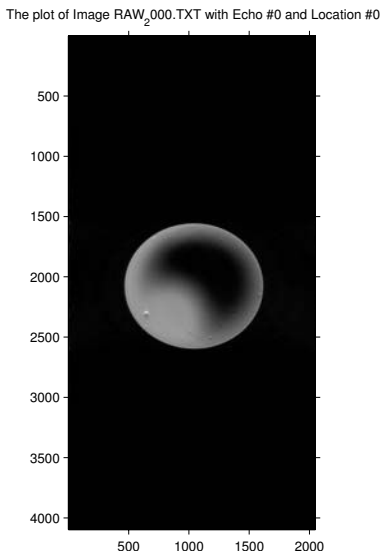

Fig. 6. Output Image using IFFT

In understanding this phenomenon, the rows and columns data in MRI K-Space can be assumed to be part of an infinitely long data sequence $X(k_x,k_y)$ which is being approximated to $X_N(k_x,k_y)$ by the application of a rectangular window function $W(\omega_{kx},\omega_{ky})$.

$$X_N(k_x,k_y) = X(k_x,k_y)W(\omega_{kx},\omega_{ky}) \quad (18)$$

where $W(\omega_{kx},\omega_{ky})$ is a rectangular window with 1 within the length $[0:N-1]$ and zero elsewhere, this is mathematically given as

$$W(\omega_{kx},\omega_{ky}) = \left\{ \begin{array}{ll} 1 & \omega_{kx},\omega_{ky} = 0,1,2,\ldots,N-1 \\ 0 & elsewhere \end{array} \right\} \quad (19)$$

Fig. 7 shows the effect of multiplying a function $X(k_x)$

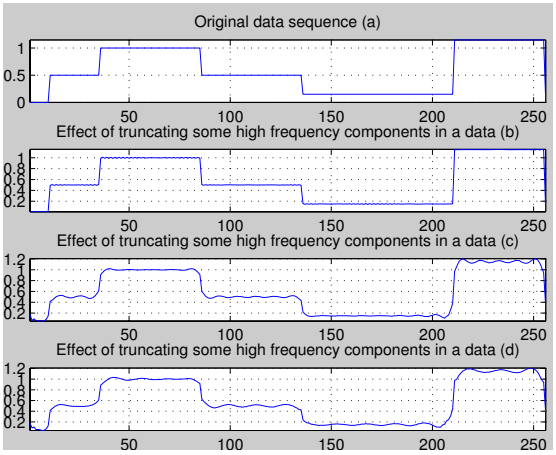

Fig. 7. GIBB'S effect in a data.(a)Original data sequence with both high and low frequency data components(b) Truncated high frequency data (c) Less severe truncated high frequency data (d)Severely truncated high frequency data

by a window $X_N(k_x)$, the ringing effect is seen to be more pronounced in Fig. 7(c) and Fig. 7(d) than in Fig. 7(b). It have been observed that as the size of the rectangular window decreases so will the approximating function continues to differs from the original function. In practical MRI data reconstruction, this effect appear in some areas of the reconstructed MR image, specially where there are sharp variations of brightness. This can be seen as dark rings around bright areas or bright rings around dark areas [6]. The problem of data truncation is more evident along the column of the data than along the rows of the data [1], [2], [6], [8].

The best way to reduce Gibb's effect is to collect more data but this is practically impossible because of time constrain and other temporal constraint. Another solution is to extrapolate some of the missing data point by the use of parametric modeling technique [1], [2], [6] and more recently the use of Artificial neural network technique [18]–[20].

B. Truncation Artifacts

In DFT analysis, the fourier transform of a rectangular window $(rect(t/\tau))$, is a sinc function $(\tau sinc(\frac{\omega\tau}{2}))$, i.e

$$rect(t/\tau) \Longleftrightarrow \tau sinc(\frac{\omega\tau}{2})$$

The sinc function sidelobes shown in Fig. 8 (a) has an appreciable amplitude and normally introduce uncertainty in the discrimination of anomical detail in the reconstructed images [6] as truncation artifacts. An image artifact is any feature which appears in an image which was not present in the original imaged object.

Solving the problem of truncation artifacts involve the use of other windowing function like Hamming, Hanning and Blackman window. These windows has lower sidelobes amplitude and provides better suppression of the oscillation at point of discontinuity compared to a rectangular window [7]. The data will be windowed prior to reconstruction and result obtained has shown that this method reduce the truncation artifacts at the expense of blurring of the output image.

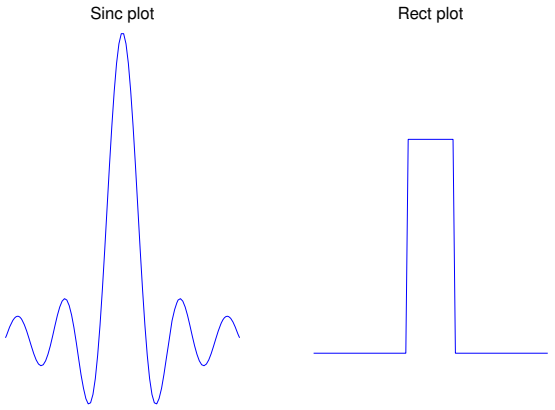

Fig. 8. Figure showing data in time domain and frequency domain (a) Sinc plot in frequency domain (b) Rect plot in time domain

Table I list some of the window functions with their time domain sequence. Also listed in the table is the value of the peak sidelobe for each of the window function.

Table II gives the measure of similarity obtained between a windowed MRI data and a model data for three different window types, namely Hamming, Hanning and Blackman window.

Result obtained shows that the use of Hamming Window produces better result when compared with other windows like Hanning and Blackman windows. Also from the result, the time for completion for Non integer power of 2 (2N Radix Image sizes) for example 512 x 178 is higher than with integer power of $2(512\text{x } 512)$. Aside truncation artifacts, there exist other sources of artifacts in MRI DFT reconstructed images. These artifacts can be as a result of improper operation of the imager, and other times a consequence of natural processes or properties of the human body and it can also be due to the image reconstruction method [4]. The most problematic physiologic motions causing artifacts in the final image include blood flow, respiratory motion, cardiac motion, and gross movements of the body.

C. Decrease in Spatial resolution

The use of DFT for MRI reconstruction leads to decrease in spatial resolution [1], [5], [6]. The windowing function used in reducing truncation artifacts and Gibb's effect tries to smooth the MRI data in order to reduce the effect of sidelobes accompanying the use of rectangular window. This effect leads to the blurring effect in the reconstructed images [6].

D. Conclusion

This paper has presented a brief overview of MR system from both hardware and instrumentation point of view. This work also gives a brief discussion on some of the basic terms associated with MR process and little explanation of the imaging equation. Furthermore, this work gives a brief tutorial on DFT and the use of DFT in MRI reconstruction. Lastly the work briefly discuss some of the associated problems with MR images obtained from the use of DFT. We hope this work

TABLE I
EFFECT OF VARIOUS WINDOW FUNCTION ON FFT DATA

Name of Window	**Time Domain Sequence** $h(n), 0 \leq n \leq M-1)$	**Peak Side-lobe (dB)**
Hamming	$0.54 - 0.46cos\frac{2\pi n}{M-1}$	-41
Hanning	$\frac{1}{2}(1 - cos\frac{2\pi n}{M-1})$	-31
Blackman	$0.42 - 0.5cos\frac{2\pi n}{M-1} + 0.08cos\frac{4\pi n}{M-1}$	-57

TABLE II
EFFECT OF VARIOUS WINDOW FUNCTION ON FFT DATA

Image size	**Window Type**	**Comp. time(sec)**	**Objective performance metrics**							
			RMSE	ADI	MDI	IFM	MSE	PSNR	SSIM	CCI
512	Hamming	9.4782	0.8088	0.2502	6.2011	0.6541	0.6541	45.061	0.9872	0.9994
x	Hanning	9.1629	0.8787	0.2711	6.7378	0.7721	0.7721	41.9091	0.9846	0.9992
178	Blackman	9.477	1.0305	0.3196	7.8893	1.0618	1.0618	35.2443	0.9778	0.9991
512	Hamming	5.751	0.5623	0.1754	4.3167	0.3633	0.3162	44.951	0.9897	0.9994
x	Hanning	5.4409	0.6109	0.1900	4.6904	0.1335	0.3732	41.838	0.9876	0.9992
256	Blackman	5.7549	0.7165	0.2238	5.4826	-0.6938	0.5133	35.162	0.9821	0.9992
512	Hamming	5.8571	0.2812	0.0876	2.1616	0.3634	0.0791	45.0631	0.9942	0.9994
x	Hanning	5.5446	0.3055	0.0950	2.3487	0.1335	0.0933	41.9558	0.9930	0.9992
512	Blackman	5.8576	0.3582	0.1118	2.7480	-0.6938	0.1283	35.2715	0.9901	0.9992
512	Hamming	6.1199	0.1406	0.0438	1.0808	0.3634	0.0198	45.0631	0.9976	0.9994
x	Hanning	5.8086	0.1527	0.0475	1.1744	0.1335	0.0233	41.955	0.9972	0.9992
1024	Blackman	6.1202	0.1791	0.0559	1.3740	-0.6938	0.0321	35.2716	0.9961	0.9992

will simulate more research interest in the area of solving some of the problems associated MR reconstruction using DFT technique.

REFERENCES

[1] Z. P. Liang and P. C. Lauterbur, "Principles of Magnetic Resonance Imaging, A signal processing perspective", IEEE Press, New York, 2000.

[2] D. G. Nishimura, "Principles of Magnetic Resonance Imaging", April 1996.

[3] E. M. Haacle and Z. P. Liang, "Challenges of Imaging Stucture and Function with MRI", *IEEE Transactions on Medicine and Biology*, Vol. 19, pp 55 - 62, 2000.

[4] "MRI Basics: MRI Basics". Accessed September 21, 2007, from Website: http://www.cis.rit.edu/htbooks/mri/inside.htm

[5] "MRI Physics: MRI Physics". Accessed May 11, 2008, from Website: http://www.mri-physics.com/

[6] M. R. Smith, S. T. Nichols, R. M. Henkelman and M. L. Wood, "Application of Autoregressive Moving Average Parametric Modeling in Magnetic Resonance Image Reconstruction", *IEEE Transactions on Medical Imaging*, Vol. M1-5:3, pp 257 - 261, 1986.

[7] F. J. Harris,"On the Use of Windows for Harmonic Analysis with the Discrete Fourier Transform", Proceedings of the IEEE. Vol. 66, January 1978.

[8] M. R. Smith, S. T. Nichols, R. Constable and R. Henkelman, "A quantitative comparison of the TERA modeling and DFT magnetic resonance image reconstruction techniques", *Magn. Reson. Med.*, Vol. 19 pp. 1-19, 1991.

[9] Z. P. Liang, F. E. Boada, R. T. Constable, E. M. Haacke, P. C. Lauterbur, and M. R. Smith, "Constrained Reconstruction Methods in MR Imaging", *Reviews of MRM*, vol. 4, pp.67 - 185, 1992.

[10] "MRI Scanner: MRI Scanner, www.magnet.fsu.edu/images/mri-scanner.jpg"

[11] Z. Hongmei, "Medical Image Processing Overview ", Lecture note, *University of Calgary*.

[12] J. Hening, "Review- article: K-space sampling strategies", *Eur. Radiol*, vol. 9, pp.1020 - 1031, 1999.

[13] E. J. Blink, " MRI: Physics", *Online PDF file*, 2004.

[14] R. C. Gonzales, Richard E. Woods, "Digital Image Processing ", second edition,. Prentice Hall, 2002.

[15] M.L Wood and R. M. Henkelman, "Truncation artifacts in magnetic Resonace Imaging ", *J. Magn. Res. Med.* Vol. 2, 1985.

[16] E. Hackle and Z. Liang, "Superresolution Reconstruction Through Object Modeling and Estimation", *IEEE transactions in A.S.S.P*, 37: 592 - 595, 1989.

[17] R. Palaniappan, "Towards Optimal Model Order Selection for Autoregressive Spectral Analysis of Mental Tasks Using Genetic Algorithm", *IJCSNS International Journal of Computer Science and Network Security*, Vol. 6 No. 1A, January 2006.

[18] H. Yan and J. Mao, "Data Truncation Artifact Reduction in MR Imaging Using a Multilayer Neural Network" *IEEE Trans. Med. Imaging* , V01.12, No. 1,pp.73-77, 1993.

[19] Y. Hui and M. R. Smith, "Comment on Data Truncalion Artifact Reduction in MR imaging Using a Multilayer Neural Networks ", *IEEE Trans. on Med. Imaging*, June 1995.

[20] Y. Hui and M. R. Smith, "MRI Reconstruction From Truncated Data Using A Complex Domain Backpropagation Neural Network", *IEEE Trans. on Med. Imaging*, June 1997.

[21] Z. Wang, A. C. Bovik, and L. Lu, "Why is image quality assessment

TABLE III
OBJECTIVE PERFORMANCE DEFINITION TABLE

Accr.	Meaning	Equation	Measure		Explanation	Ref.
			Min. value	Max. Value		
MSE	Mean square error	$\frac{1}{MN}\sum_{m=1}^{M}\sum_{n=1}^{N}\|U(m,n)-V(m,n)\|^2$	0	1	Lower value signify closeness	[21], [23], [29], [30]
RMSE	Root Mean Square	$\sqrt{MSE}$	0	1	Lower value signify closeness	[23], [29], [30]
ADI	Average difference indicator	$\frac{1}{MN}\sum_{m=1}^{M}\sum_{n=1}^{N}(U(m,n)-V(m,n))$	0	1	Lower value signify closeness	[31]
MDI	Maximum difference indicator	$Max(\|U(m,n)-V(m,n)\|)$	0	1	Lower value signify closeness	[31]
IFM	Image fidelity measures	$1-\frac{\sum_{m=1}^{M}\sum_{n=1}^{N}\|U(m,n)-V(m,n)\|^2}{\sum_{m=1}^{M}\sum_{n=1}^{N}(U(m,n))^2}$	0	1	Lower value signify closeness	[31]
PSNR	Peak to signal noise ratio	$20log_{10}\frac{Max(V(m,n))}{RMSE}$	0	∞	Higher value of PSNR indicates that the two images are similar	[29], [30]
SSIM	Structural similarity	$\frac{4\rho_{u,v}\bar{U}\bar{V}}{(\rho_u^2)+\rho_v^2)[\bar{U}^2+\bar{V}^2]}$	0	1	1 shows that the images are similar to each other	[21], [23], [24], [29]
CCI	Correlation coefficients index	$\frac{\sum_{m=1}^{M}\sum_{n=1}^{N}[U(m,n)-\bar{U}][(V(m,n)-\bar{V}]}{\sqrt{\sum_{m=1}^{M}\sum_{n=1}^{N}[U(m,n)-\bar{U}]^2\sum_{m=1}^{M}\sum_{n=1}^{N}[V(m,n)-\bar{V}]^2}}$	-1	+1	1 indicate that the two images are highly similar while -1 indicate that the two images are exactly opposite	[30]

so difficult", *Proc. IEEE Int. Conf. Acoustics, Speech, and Signal Processing*, vol.4, Orlando, FL, pp. 3313-3316, May, 2002.

[22] T. Mathews Jr. and M. R. Smith, "Objective Image Quality Measures for Evaluating Advanced MRI Reconstruction Method", *Proc. of IEEE CCECE*, pp. 396 - 361, 1996.

[23] Z. Wang and A. Bovik, "A Universal quality index", *IEEE Signal Processing Letters*, vol. 9, no. 3, pp. 8 1-84, March 2002.

[24] Z. Wang, A. C. Bovik, H. R. Sheikh, and E. P. Simoncelli, "Image quality assessment:From error measurement to structural similarity", *IEEE Transactions on Image Processing*, accepted for publication April 2003.

[25] H. Akaike, "Power Spectrum Estimation through Autoregression Model Fitting", *Annals of the Institute of Statistical Mathematics*, vol. 21, pp. 407-419, 1969.

[26] H. Akaike, "A New Look at the Statistical Model Identification", IEEE Trans. Autom. Control, vol. AC-19, pp. 716-723, 1974.

[27] J. Rissanen, "Modelling by shortest data description", Automatica, vol.14, pp.465-471, 1978.

[28] M.J. Salami, A. R. Najeeb, O. Khalifa and K. Arrifin, "MR Reconsturction with Autoregressive Moving Average", *International Conference on Biotechnology Engineering*, Kuala Lumpur, pp 676 - 704, May, 2007.

[29] G. P. Mulopulos, A. A. Hernandez and L. S. Gasztonyi "Peak Signal to Noise Ratio Performance Comparison of JPEG and JPEG 2000 for Various Medical Image Modalities" , Symposium on Computer June, 2003.

[30] B. Shrestha, C.G. O'Hara and N. H. Younan, "JPEG2000: IMAGE QUALITY METRICS", ASPRS 2005 Annual Conference, Baltimore, Maryland March 7-11, 2005.

[31] A. M, Eskicioglu and P. S. Fisher, P. S, "Image quality measures and their performance", *IEEE Transaction on Communications*, 43(12): 2959 - 2965, 1995.